Helicenes grafted with 1,1,4,4-tetracyanobutadiene moieties pi-helical push-pull systems with strong electronic circular dichroism and two-photon absorption

Romain Bouvier, Raphaël Durand, Ludovic Favereau, Monika Srebro-Hooper, Vincent Dorcet, Thierry Roisnel, Nicolas Vanthuyne, Yuly Vesga, Julie Donnelly, Florencio Hernandez, et al.

10.1002/chem.201802763

WILEY-VCH

Helicenes grafted with 1,1,4,4-tetracyanobutadiene moieties: π-helical push-pull systems with strong electronic circular dichroism and two-photon absorption

Romain Bouvier,[a] Raphaël Durand,[a] Ludovic Favereau,[a] Monika Srebro-Hooper,[b] Vincent Dorcet,[a] Thierry Roisnel,[a] Nicolas Vanthuyne,[c] Yuly Vesga,[d] Julie Donnelly, [d] Florencio Hernandez,[d] Jochen Autschbach,*[e] Yann Trolez,*[a] and Jeanne Crassous*[a]

Dedication ((optional))

Abstract: Enantiopure *P*- and *M*-carbo[6]helicenes substituted with one or two tetracyanobutadienes in positions 2 and 15 have been prepared. Grafting of these accepting groups on the π-helical core resulted in strong charge transfer effects which highly affected UV-visible, electronic circular dichroism and two-photon absorption responses. The ECD signal was found to be reversibly switched by applying a redox stimulus.

Introduction

Designing chiral molecular materials with strong chiroptical properties has attracted considerable attention in the last decades due to their specific interaction with polarized light. [1,2] Indeed, the possibility to tune optical rotation (OR), electronic circular dichroism (ECD), and circularly polarized luminescence (CPL) is especially appealing since it may find applications in different fields of science such as information transport and storage, optical displays, logic gates, and biology.[3] In this regard, [*n*]helicene derivatives have appeared as ideal molecular candidates because of their peculiar chiral π-conjugated helical structure which provides them with high racemization barrier (especially for $n \geq 6$), large-magnitude OR, and intense ECD and CPL signatures.[4] Their recent implementation in circularly polarized organic light emitting diodes (CP-OLEDs),[5] organic transistors,[6] and organic photovoltaic cells[7] have opened new perspectives for chirality and chiroptical materials in materials science. Aside from linear chiroptics, helicenes have recently shown to exhibit two-photon circular dichroism (TPCD).[8] Finally, chiroptical switching of helicenes using light, acid/base, or redox stimuli represents another attractive area for developing potential molecular memory elements or logic operators for data storage.[9]

1,1,4,4-Tetracyanobutadienes (TCBDs) are known to be strongly accepting groups that may give rise to donor-acceptor (push-pull) molecular structures when conjugated to donor fragments, and provide remarkably strong one-photon absorption in the visible and red region, along with nonlinear optical responses.[10a,b] TCBDs possess electron-accepting properties that are able to significantly tune absorption features of molecules and, more generally, have a strong impact on the physical characteristics of the moieties they are linked to.[10] Their synthesis implies a sequence of [2+2] cycloaddition-retroelectrocyclization (CA-RE) between tetracyanoethylene (TCNE) and electron-rich alkynes activated by donating groups.[11] The identity of these donors is various and the yield of the reaction strongly depends on their nature. Some years ago, some of us reported the synthesis of TCBDs from ynamides, which played the role of electron-rich alkynes.[12a,b] Their reduction potentials were among the lowest out of reported so far TCBDs, allowing us to envisage promising applications by tuning properties of extended π-systems. Accordingly, we wanted to investigate the influence of TCBDs coming from ynamides on the physical and (chiro)optoelectronic properties of helicenes.

Herein, we thus report on the synthesis of multifunctional chiral molecules resulting from the conjugation between a helicenic core and one or two electron-withdrawing TCBD units (Figure 1). Thanks to the synergic effect between the π-helix and the TCBD units, these enantiopure molecules displayed linear absorption and ECD in the visible region together with nonlinear two-photon absorption (TPA) response. Their UV-vis, ECD, and TPA spectral features were rationalized by quantum-chemical calculations. The potential use of these systems as redox-triggered chiroptical switches was also examined.

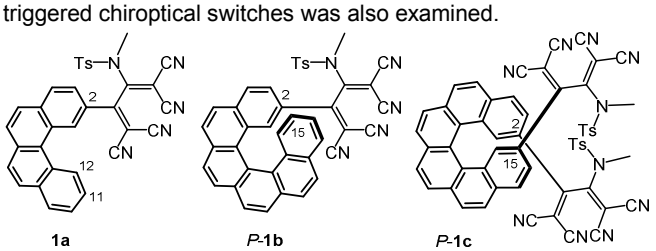

Figure 1. Chemical structures of carbo[4] and carbo[6]helicene-TCBD derivatives **1a** and *P*-**1b,c**. Ts = tosyl.

[a] R. Bouvier, R. Durand, Dr. L. Favereau, Dr. V. Dorcet, Dr. T. Roisnel, Dr. Y. Trolez, Dr. J. Crassous
Univ Rennes, Ecole Nationale Supérieure de Chimie de Rennes, CNRS, ISCR – UMR6226, F-35000, Rennes, France.
E-mail: yann.trolez@univ-rennes1.fr, jeanne.crassous@univ-rennes1.fr
[b] Dr. M. Srebro-Hooper, Faculty of Chemistry, Jagiellonian University, Gronostajowa 2, 30-387 Krakow, Poland.
[c] Dr. N. Vanthuyne, Aix Marseille University, CNRS, Centrale Marseille, iSm2, Marseille, France.
[d] Y. Vesga, J. Donnelly, Prof. F. Hernandez, Department of Chemistry, The College of Optics and Photonics, CREOL, University of Central Florida, Orlando, FL 32816-2366, USA.
[e] Prof. J. Autschbach, Department of Chemistry, University at Buffalo, State University of New York, Buffalo, NY 14260, USA. E-mail: jochena@buffalo.edu

Supporting information for this article is given via a link at the end of the document.((Please delete this text if not appropriate))

Results and Discussion

Synthesis of mono- and bis-substituted helicene-TCBD derivatives 1a-c

We first decided to evaluate the possibility to synthesize an ynamide conjugated with a polycyclic aromatic structure, namely a benzophenanthrene, and to make it react with TCNE to obtain derivative **1a** (Figure 1). To do so (Scheme 1, top), compound **2a** was prepared according to a described procedure[13a] and reacted with *N*-bromosuccinimide (NBS) in the presence of a catalytic amount of silver nitrate to give carbo[4]helicene-ethynylbromide **3a** with 77% yield. Then, **3a** was subjected to Hsung conditions[12c] to form ynamide **4a** with modest 26% yield (unoptimized due to the very low solubility of **3a**). Reacting **3a** with TCNE *via* a [2+2] cycloaddition followed by a retro-electrocyclization[12a,b] (CA-RE sequence) finally afforded the target carbo[4]helicene-TCBD derivative **1a** with 99% yield. The compound was fully characterized; its ^{1}H NMR displayed the typical signals for both the [4]helicenic core (see Supplementary Information, SI) with for instance the two typical down-field shielded H^{11} and H^{12} at 9.33 and 8.96 ppm, respectively; its ^{13}C NMR spectrum showed the characteristic peaks of the four cyano groups resonating between 110 and 113 ppm, indicating the unambiguous presence of the TCBD moiety.

The successful synthesis of **1a** encouraged us to prepare longer and configurationally stable carbo[6]helicene-TCBD derivatives. The same synthetic approach, *i.e. i*) bromination of the triple bond, *ii*) Hsung coupling,[12c] and *iii*) CA-RE sequence, was therefore applied to mono-2-trimethylsilylethynyl- (*rac*-, *P*- or *M*-**2b**)[13b] and bis-2,15-trimethylsilylethynyl-carbo[6]helicene (*rac*-, *P*- or *M*-**2c**)[13b] to obtain respectively compounds **1b** and **1c** in either racemic, or enantiopure *P* and *M* forms, with good overall yields (Scheme 1, middle and bottom). These compounds were also fully characterized by NMR spectroscopy and mass spectrometry (see SI). For instance, while the ^{1}H NMR of C_1-symmetric **1b** displayed the characteristic methyl groups at 2.34 and 2.57 ppm, a typical up-field shielded ddd signal at 6.82 ppm corresponding to H^{15} (see Figure 1) was found. Regarding C_2-symmetric **1c**, its higher symmetry was reflected in its much simpler ^{1}H-NMR spectrum.

Since crystals of *rac*-**1b**, *P*-**1b** and of *rac*-**1c** could be grown by slow diffusion of pentane vapors onto dichloromethane solutions, the structures of **1b** and **1c** could also be ascertained by X-ray crystallography (see Figure 2 for *rac*-**1b**,**c** and SI). The *rac*-**1b**, *P*-**1b** and *rac*-**1c** compounds crystallized in the *P*-1, $P6_122$ and *C*2/c space groups and displayed helicity (dihedral angle between the terminal helicenic rings) of 57.9, 59.7 and 61.2°, respectively, that are within the range of classical carbo[6]helicenes.[4] Regarding the TCBD units, the two dicyanovinyl fragments form a dihedral angle of 62.8, 89.2 and 57.5° for *rac*-**1b**, *P*-**1b** and *rac*-**1c**, respectively, thus showing classical strong distortions.[10] However, in each derivative, one of the two dicyanovinyl branch is nearly coplanar with the helicene terminal ring (dihedral angle lower than 17°) therefore ensuring efficient conjugation with the π-helical core (see Figures 2a,b). On the contrary, the tosyl groups are all placed out of the terminal helicenic planes and are involved in the supramolecular organization through π–π interactions. Indeed, in Figures 2c and 2d,e are depicted the homochiral and heterochiral assemblies of *P*-**1b** and *rac*-**1c**, respectively. *P*-**1b** displays a dimeric homochiral arrangement with intermolecular π–π interactions between the *P* enantiomers and intramolecular π–π stacking between the phenyl of the tosyl group and the closer terminal helicenic ring (centroid-centroid distance of 3.64 Å, Figure 2c). *Rac*-**1c** organizes into repeated supramolecular motifs with intermolecular π–π interactions occuring between *i*) the helicenic cores and *ii*) TCBD tosyl units of *P* and *M* enantiomers (Figures 2d,e).

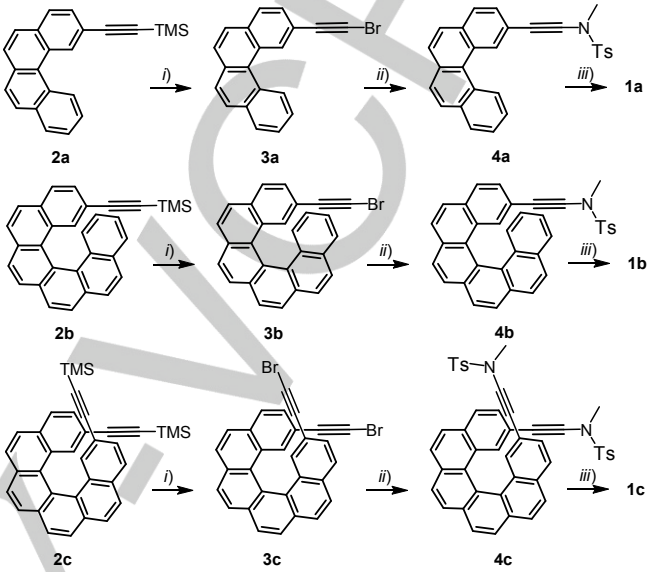

Scheme 1. Synthesis of derivatives **1a** and *rac*-, *P*- or *M*-**1b**,**c** from **2a** and *rac*-, *P*- or *M*-**2b**,**c**, respectively. *i*) NBS, cat. $AgNO_3$, acetone, 77% to quant.; *ii*) TsNHMe, $CuSO_4{\cdot}5H_2O$, 1,10-phenanthroline, K_3PO_4, toluene, 90°C, Ar, 18h, 26% to quant.; *iii*) TCNE, CH_2Cl_2, 18h, 62-90%. Compounds of series **b** and **c** are obtained in racemic and enantiopure forms.

UV-vis spectroscopy

UV-vis one-photon absorption spectra of **1a**-**c** were recorded in dichloromethane solutions and are displayed in Figure 3 along with the absorption spectrum of bis-trimethylsilyl-ethynyl-helicene precursor **2c**.[14a] The functionalization of the carbo[4] or carbo[6]helicene core by one or two TCBD unit(s) strongly modifies its absorption spectrum with the appearance of new broad and intense visible bands between 390 and 550 nm. These additional bands can be attributed to a strong intramolecular charge transfer (ICT) from the π-electron system of the helicenic donor fragment to the TCBD group(s), as previously observed for other TCBD-based derivatives,[10-12] and as demonstrated here by TDDFT calculations and electrochemistry.[15] Indeed, the simulated (BHLYP with the continuum solvent model for dichloromethane) UV-vis spectra agree well with the experiment and confirm helicene-to-TCBD ICT character of the additional absorption at 460 nm in **1b**,**c** (Figures 4 and 5, Table 1, SI). Namely, the lowest-energy excitation with sizeable oscillator strength in **1b**, #2 calculated at 482 nm, corresponds to transitions from the two highest occupied (HO) molecular orbitals (MOs) to the lowest unoccupied (LU) MO, with the occupied orbitals localized on the π-helical core and LUMO spread out mainly over the π-electron system of the TCBD group (with almost no contribution of the *N*-tosyl unit). For **1c**, the lowest-energy UV-vis band originates predominantly from three excitations close in energy, #1 calculated at 460 nm, #2 at 456 nm, and #4 at 431 nm, which

involve contributions from nearly degenerate helicene-centered HOMO-1, HOMO and TCBD-centered LUMO, LUMO+1. Note that HOMO-1 and HOMO of **1c** represent two distinct π-orbitals of the helicene electron system, while LUMO and LUMO+1 represent in-phase and out-of-phase linear combinations of the lowest unoccupied TCBD frontier molecular fragment orbitals (FOs, *vide infra*). Furthermore, the small energetic splitting between LUMO and LUMO+1 indicates that the TCBD-centered LUFO π-orbitals of **1c** weakly interact with each other through the helicene.

As shown in Figure 3, a visible red-shift of the lowest-energy intensity, from 420 to 480 nm, but without change in the molar extinction coefficients ($\varepsilon \sim 5 \times 10^3$ M^{-1} cm^{-1}) is observed for **1b** as compared to **1a**, which can be explained by an extension of the conjugated π-electron system for **1b**. On the contrary, the corresponding band in **1c** appears to be blue-shifted (by ca. ~ 50 nm) and strongly enhanced in intensity (molar extinction coefficient increased by a factor of two at 420 nm) relative to **1b**. Both these features are well reproduced by the calculations. Inspection of the orbital energies (see Figure 5) reveals noticeable energetic stabilization of the high-lying occupied orbitals and almost no effect on the lowest unoccupied TCBD-centered MOs upon introduction of two TCBD units onto helicene core comparing to the mono-substituted system. This results in an increase in HOMO-1,HOMO–LUMO,LUMO+1 gap(s) for **1c** that may rationalize the observed blue-shift of its low-energy ICT band. The corresponding increase in the intensity of this band can be attributed to the overlapping of dual ICT absorption from the helicene to the two TCBD units (*vide supra*) and exciton coupling interactions between those ICT states (*vide infra*).

ECD spectroscopy

The effect of the strong charge transfers in helicene-TCBD systems **1b**,**c** is particularly striking in their ECD spectra (see Figure 3). Indeed, while the precursor *P*-**2c** displays a negative ECD band at 280 nm ($\Delta\varepsilon$ = - 224 M^{-1} cm^{-1}) and a positive one at 341 nm ($\Delta\varepsilon$ = + 320 M^{-1} cm^{-1}) that are typical for helicene derivatives and correspond to the classical π–π* transitions (see Ref. [14a]), *P*-**1b** and *P*-**1c** show two negative bands at 243 nm ($\Delta\varepsilon$ = -188 M^{-1} cm^{-1} for **1b**,**c**) and 300 nm (**1b**: $\Delta\varepsilon$ = -34 M^{-1} cm^{-1}, **1c**: $\Delta\varepsilon$ = -97 M^{-1} cm^{-1}), and one positive ECD band between 340-346 nm ($\Delta\varepsilon$ = +125 M^{-1} cm^{-1} for **1b**,**c**). In line with the UV-vis absorption, *P*-**1b**,**c** demonstrate also additional ECD bands between 390-550 nm, much more intense and with a bisignate signature ($\Delta\varepsilon$ = -10 M^{-1} cm^{-1} at 397 nm and +55 M^{-1} cm^{-1} at 480 nm) in the bis-substituted *P*-**1c** system as compared to the mono-substituted *P*-**1b** derivative ($\Delta\varepsilon$ = +14 M^{-1} cm^{-1} at 480 nm) (see inset of Figure 3).

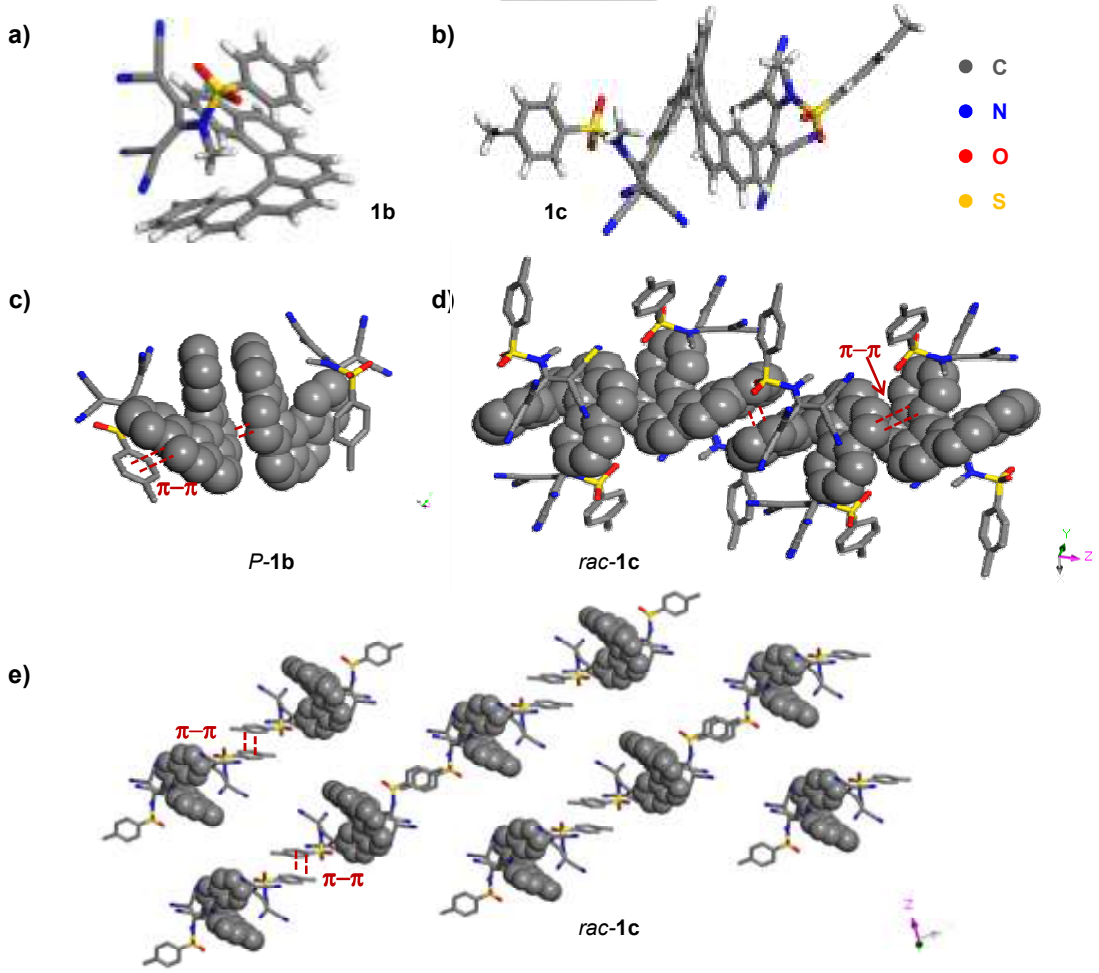

10.1002/chem.201802763

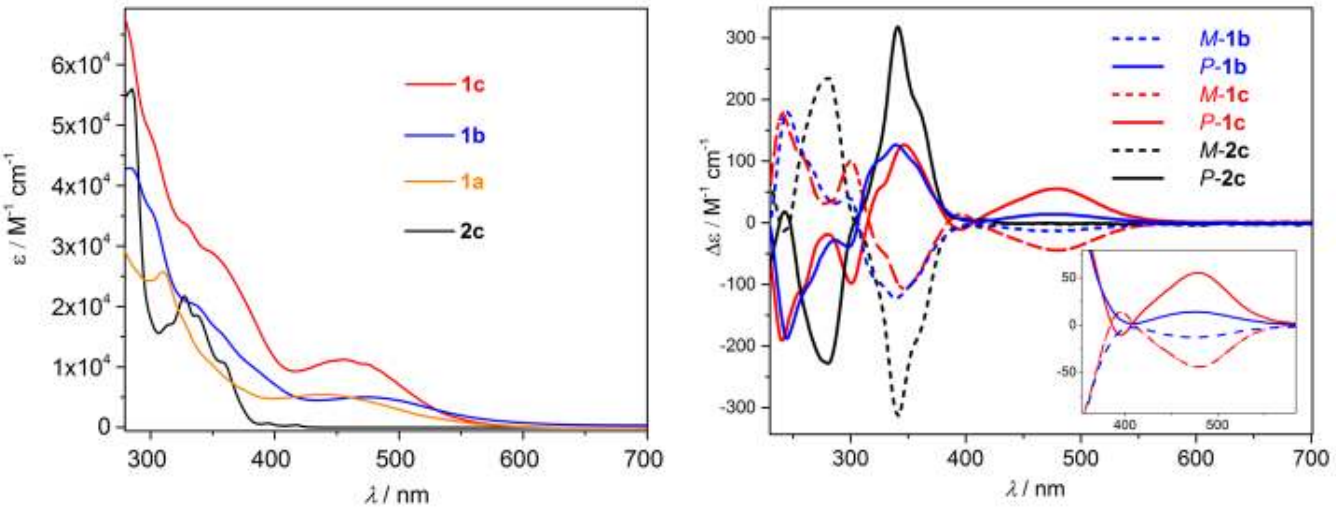

Figure 3. Left: UV-vis spectra of bis-trimethylsilyl-ethynyl-helicene precursor **2c** (black), and helicene-TCBD derivatives **1a** (orange), **1b** (blue), and **1c** (red) (dichloromethane, 298 K, *C* 10^{-5} M). Right: Mirror-image ECD spectra of enantiopure *P*- and *M*-**1b**,**c** compared to *P*- and *M*-**2c**.

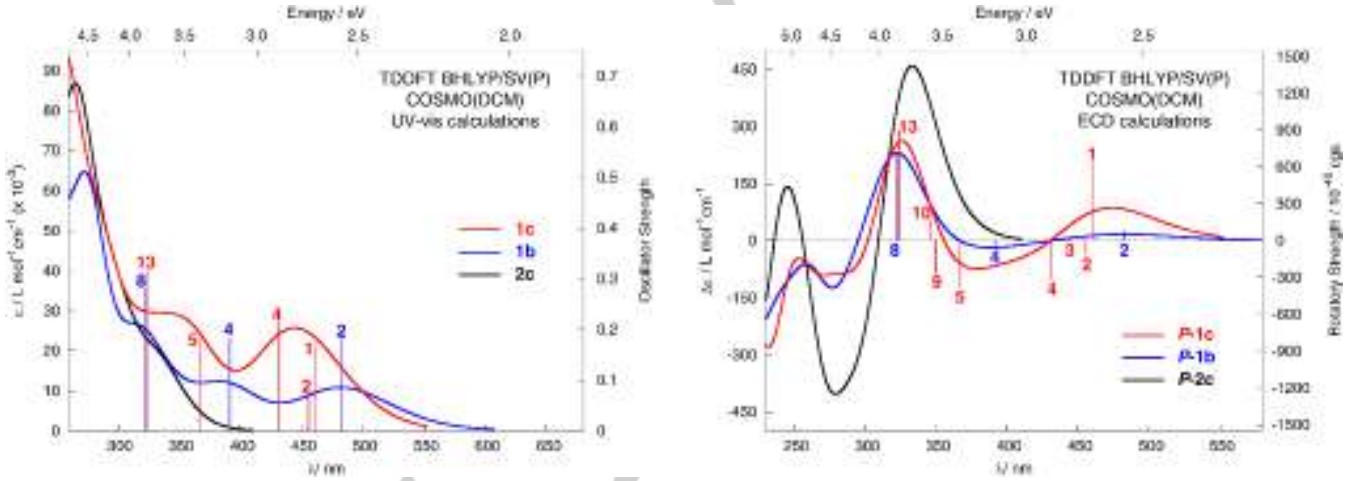

Figure 4. Comparison of the simulated UV-vis (left) and ECD (right) spectra of helicene-TCBD derivatives *P*-**1b,c** with bis-trimethylsilyl-ethynyl-helicene system *P*-**2c** used as a reference. No spectral shift has been applied. Calculated excitation energies and rotatory strengths indicated as 'stick' spectra. Numbered excitations correspond to those analyzed in detail. For the assignment of the calculated spectra of **2c** see Ref. [14a]. See also SI.

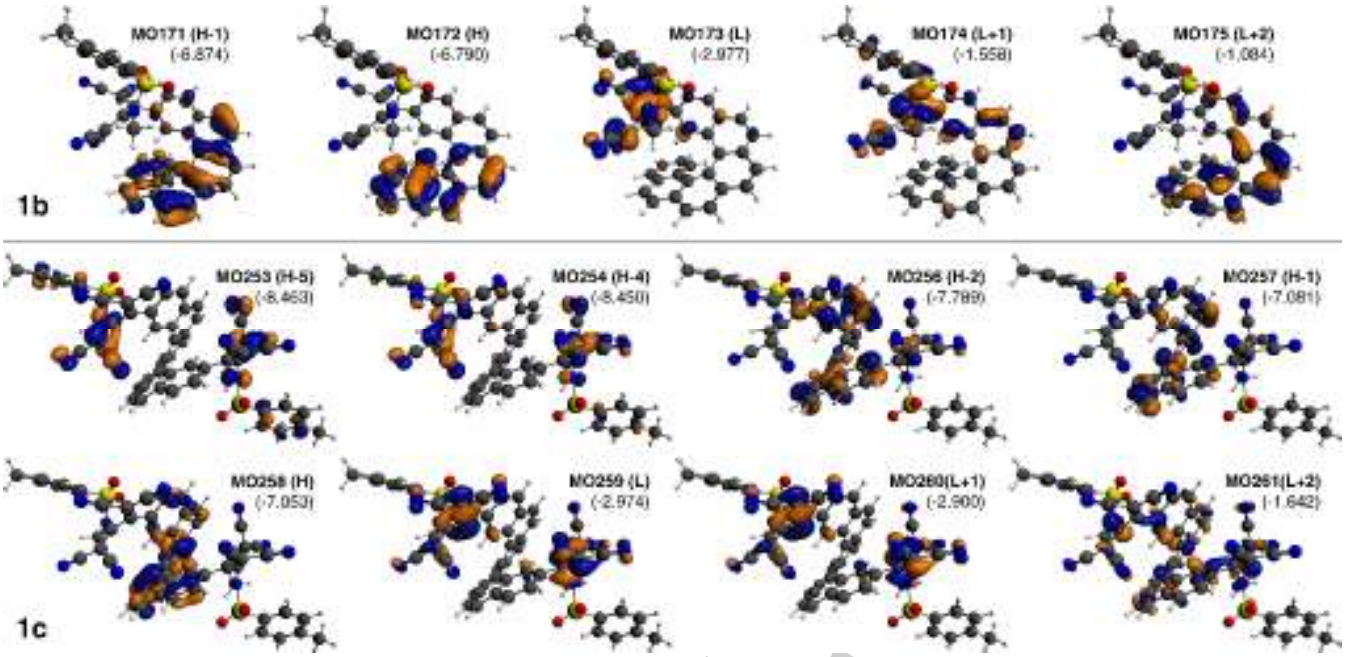

Figure 5. Isosurfaces (±0.04 au) of MOs involved in selected transitions of **1b** (top) and **1c** (bottom). 'H' = HOMO, 'L' = LUMO. Values listed in the parentheses are the corresponding orbital energies, in eV. See also SI.

Table 1. Selected dominant excitations and occupied (occ) – unoccupied (unocc) MO pair contributions (greater than 10%) of the *P*-**1b** and *P*-**1c**. See also SI.

	Excitation	*E* / eV	λ / nm	*f*	*R* / 10^{-40} cgs	occ no.	unocc no.	%
P-**1b**	#2	2.57	482	0.182	80.77	171	173	83.8
						172	173	11.1
	#4	3.17	391	0.182	-64.27	170	173	56.2
						169	173	32.6
	#8	3.86	321	0.280	717.92	172	175	40.3
						171	174	27.2
						172	176	18.8
P-**1c**	#1	2.69	460	0.170	641.85	257	259	54.7
						258	260	34.8
	#2	2.72	456	0.067	-117.63	258	259	91.0
	#3	2.80	443	0.036	30.76	258	260	56.7
						257	259	36.1
	#4	2.88	431	0.215	-318.23	257	260	89.9
	#5	3.38	367	0.182	-384.31	256	259	86.1
	#9	3.54	350	0.105	-269.53	254	259	32.9
						253	260	28.5
						257	261	15.1
	#10	3.59	346	0.022	176.42	254	260	28.1
						253	259	28.1
						255	260	26.8
	#13	3.83	323	0.318	900.83	257	261	43.7

258	262	32.5

The ECD envelopes for helicene-TCBD derivatives *P*-**1b**,**c** and the reference system *P*-**2c** calculated with linear response TDDFT (BHLYP functional) reproduce, in general, very well the experimentally observed ECD features (Figure 4). The analysis of molecular orbital pair-contributions to selected dominant excitations for *P*-**1b**,**c** (Figures 4 and 5, Table 1, SI) shows that the main positive intense band of these systems observed experimentally around 340 nm originates mainly, as expected, from helicene-centered π-π* excitations (see excitation #8 calculated at 321 nm for *P*-**1b** and excitation #13 calculated at 323 nm for *P*-**1c**). However, the unoccupied MOs involved in those excitations spread out also over the TCBD π-systems (see for example LUMO+1 for **1b** and LUMO+2 for **1c** in Figure 5), and therefore these excitations afford a partial helicene-to-TCBD charge-transfer character.

In line with the experiment, additional low-energy ECD bands attributed to strong ICTs from the π-electron system of the helicene core to the TCBD group(s) are also visible in the simulated spectra of *P*-**1b**,**c**. In the case of *P*-**1b** the aforementioned excitation #2 (calculated at 482 nm) and excitation #4 (391 nm) reveal opposite-sign rotatory strengths (*R*) and consequently lead to the appearance of a bisignate pair of bands in the low-energy part of the simulated ECD spectrum. The rotatory strength of excitation #4 appears to be overestimated in the calculations as the corresponding experimental ECD of *P*-**1b** does not become negative in this energy region. An analogous but much more intense bisignate ECD is computed for *P*-**1c** due to four intense excitations: #1 at 460 nm has positive *R* while excitations #2 (456 nm), #4 (431 nm), and #5 (367 nm) have negative *R*. The strong intensity of excitation #5, which is evidently not suppressed sufficiently by the positive ECD intensity of higher-energy excitations, may be responsible for the overestimation of the negative band around 400 nm for *P*-**1c** when comparing with the experiment. Note that the intensity of the negative band for both *P*-**1b** and *P*-**1c** seems to be very sensitive to the solvent effects (see SI).

Of particular interest is the possibility of exciton coupling (EC) ECD for the bis-substituted helicene-TCBD **1c**. We discuss this system in relation to a carbo[6]helicene functionalized with two diketopyrrolopyrrole (DPP) groups, for which we recently clearly demonstrated EC ECD and corresponding CPL in the low-energy (long-wavelength) region.[14a] The TCBD-N(Me)(Ts) substituent differs in crucial ways from DPP in that its frontier molecular FOs are much lower in energy overall, namely 2.3 and 0.9 eV lower than for DPPBr for the HOFO and LUFO, respectively, and there is also a 1.4 eV larger energy gap between these FOs (BHLYP calculations, see SI). This has two important consequences.

First, the much smaller frontier FO energy gap for the DPP substituent allows for electronic excitations with strong EC ECD character at 2.2 eV (560 nm), which is well below the energies of any of the helicene-centered transitions. For **1c**, due to the larger FO energy gap a typical substituent-centered exciton couplet appears around 3.5 eV (ca. 350 nm, excitations #9 and #10) with a -/+ sign pattern when going from lower to higher energy (see Figure 4 and Table 1). The occupied MOs involved in this exciton couplet are nos. 253 and 254 (see Figure 5) which clearly represent in-phase and out-of-phase linear combinations of the HOFOs of TCBD, while the participating unoccupied MOs are the aforementioned LUMO and LUMO+1 corresponding to linear combinations of the TCBD LUFOs. The energies of the excitations and the participating MOs are consistent with an exciton coupling of the HOFO-LUFO transitions of the substituents. However, the presence of the couplet is hardly visible in the broadened ECD spectrum. The couplet is overpowered by the pair of excitations no. 5 and 13 at lower and higher energy, respectively, which have the same -/+ sign pattern of their rotatory strengths as the exciton couplet.

Second, the low energy of the lowest unoccupied FO renders TCBD an ideal acceptor group in ICT excitations. This is clearly seen in the assignment of the long-wavelength excitations of both **1b** (#2 and #4) and **1c** (#1, #2, #4, and #5) in which the participating orbitals are the three highest occupied helicene π-orbitals (HOMO-2 to HOMO) and the TCBD-centered LUMO (for **1b**) or LUMO, LUMO+1 (for **1c**). Due to the ICT character, these excitations have sizable and similar dipole strengths for both **1b** and **1c**. However, for **1b** the corresponding rotatory strengths are weak, whereas the ECD intensity of *P*-**1c** is drastically enhanced in this region of the spectrum.

It therefore appears that the ECD-intense long-wavelength excitations of **1c** can be conceptualized as an exciton coupling among transitions from helicene π-orbitals to the lowest unoccupied FO of either one of the TCBD substituents. Due to the rigidity and chirality of the helicene, the associated un-coupled electric transition dipoles form a helical arrangement, similar to the un-coupled transition dipoles in a traditional EC ECD couplet, resulting in the fairly intense ECD of **1c** between 550 and 350 nm. We note that the role of charge transfer states in EC models is well recognized.[16] The case of **1c** is somewhat less typical in that the ICT transitions that couple together originate in the same subsystem, namely the helicene. The physical mechanism causing the long-wavelength ECD intensity is however likely the same as in traditional exciton coupling CD, namely an electrostatic coupling of two or more electric transition dipoles with accompanying magnetic transition dipoles coupled in a helical arrangement.

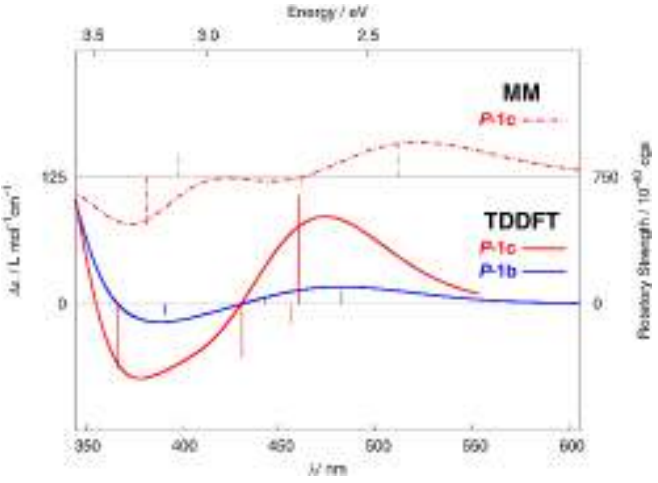

Figure 6. Comparison of low-energy region of ECD spectra for *P*-**1b** and *P*-**1c** from TDDFT BHLYP calculations and from matrix method dipole coupling model.

In order to verify the hypothesis that the origin of the intense long-wavelength ECD of **1c** is due to a coupling of individual helicene-to-TCBD electric transition dipole moments (TDMs) resulting in rotatory strengths that are much larger than those of the un-coupled transitions, a 'matrix method' (MM) dipole coupling model[17] as described in Ref. [17b] was set up, with the energies and TDMs for excitations #2 and #4 of mono-substituted helicene-TCBD **1b** as input. Further details can be found in the SI. Figure 6 compares the resulting MM spectrum with the TDDFT calculated ones for **1c** and **1b**. Despite its simplicity, the model is consistent with a positive/negative ECD when going from longer to shorter wavelengths as a result of excitonic electric TDM coupling of individual helicene π to TCBD π^* transitions. The long-wavelength ECD of **1c** is further enhanced, relative to the dipole coupling model, and blue-shifted, by the electronic coupling between the helicene core and the substituents, similar to what we found recently for the bis-substituted helicene-DPP system.[14a]

It therefore appears that the long-wavelength chiroptical properties of helicenes can be tuned and enhanced by functionalization with different types of groups. Strongly absorbing substituents such as DPP then gives rise to helicene-enhanced exciton coupling ECD and luminescence, while strong electron acceptors such as TCBD promote helicene-enhanced ECD due to exciton coupling of charge-transfer excitations originating in the helicene π-system, thus describing a kind of exciton coupling within a helical push-pull system.[11e,14] While, such spectral effects may also have been observed previously,[14d] no specific distinctions were made between standard vs. ICT EC. Note that contrary to helicene-DPP systems which are chiral emitters in solution, the helicene-TCBD derivatives are not emissive, neither in solution nor in the solid state.

Electrochemical behavior and chiroptical redox switching

Several examples of chiroptical switching properties based on redox-active organometallic or heteroatomic helicenic derivatives have been reported in the literature,[9] but only limited examples have shown reversible reductive behavior.[18] The redox properties of the acceptor-substituted helicene-TCBDs **1a-c** were studied using cyclic voltammetry (CV) in dichloromethane with nBu$_4$NPF$_6$ (0.1 M) as the supporting electrolyte, *vs.* saturated calomel electrode (SCE) (see Table 2 and Figure S1.7 in the SI). The mono-substituted systems **1a,b** show two reversible, well-resolved 1e$^-$ reduction steps centered on the tetracyanobutadiene unit at *ca.* -0.16 and -0.70 V *vs.* SCE, while the bis-substituted **1c** displays four reversible 1e$^-$ reductions, with the third and fourth ones being very close in potential. These data are in agreement with the results obtained for formerly studied TCBD derivatives.[11,12] The fact that **1c** exhibits a difference of 230 mV between the first and second reduction processes indicates either a significant electronic interaction between the two mono-reduced TCBD fragments inside the helical environment, which may be explained by a gain of electron density on the helicene core after the first reduction event or the presence of Coulombic repulsion between negatively charged units. These effects become negligible when the TCBD units are doubly reduced (ΔE_{Red} = 60 mV between E_{Red3} and E_{Red4}, see Table 2 and SI).

Table 2. Redox potentials (E_{Red}) of **1a**, **1b** and **1c** compounds referenced *versus* SCE and given in V (scanning rate: 100 mV s^{-1}).

Compound	E_{Red} (V)
1a	-0.15, -0.66
1b	-0.18, -0.73
1c	-0.17, -0.40, -0.72[a], -0.78[a]

[a] Determinated by differential pulse voltammetry (step potential: 10 mV)

Taking advantage of the reversibility of the redox processes in combination with the strong ECD response of the helicene-TCBD **1c** in the visible region, we examined its redox-triggered ECD switching activity. First, we evidenced the UV-vis signatures of the reduced **1c** species, i.e. **1c**$^-$, **1c**$^{2-}$, and **1c**$^{4-}$, by spectroelectrochemical studies. As depicted in the left panel of Figure 7, **1c**$^-$ and **1c**$^{2-}$ exhibit very similar absorption spectra, slightly modified as compared to the neutral system **1c** by (1) the appearance of a new band between 550 and 700 nm, (2) a small red-shift and increase in the intensity of **1c** initial band centered at 450 nm, and (3) an absorption decrease around 355 nm, resulting in an isosbestic point at 390 nm. Since the third and fourth reduction of **1c** occur at almost similar potentials, we directly monitored the spectra of **1c**$^{4-}$ which shows, relative to **1c**$^{2-}$, a further increase in the absorption between 550 and 750 nm, a 30 nm red-shift of the band at 470 nm, and an intensity decrease around 385 nm. Isosbestic points were observed at 350 and 493 nm (see Figure S1.8), which ascertain the continuous stoichiometry when going from **1c**$^{2-}$ to **1c**$^{4-}$ during the spectroelectrochemical experiment. In addition, the stability of **1c**$^{2-}$ and **1c**$^{4-}$ and their reversible interconversion with **1c** were evaluated by switching the applied potential (*vs.* SCE) between 0 and -0.4 V (**1c** ↔ **1c**$^{2-}$) and between 0 and -1.0 V (**1c**$^{2-}$ ↔ **1c**$^{4-}$) while recording the resulting UV-vis absorption at one defined wavelength. This switching experiment showed that redox-induced conversion between **1c** and **1c**$^{2-}$ was fully reversible (see right panel of Figure 7), while the corresponding process between **1c** and **1c**$^{4-}$ appeared to be less reversible due to the instability of the latter under our experimental conditions.

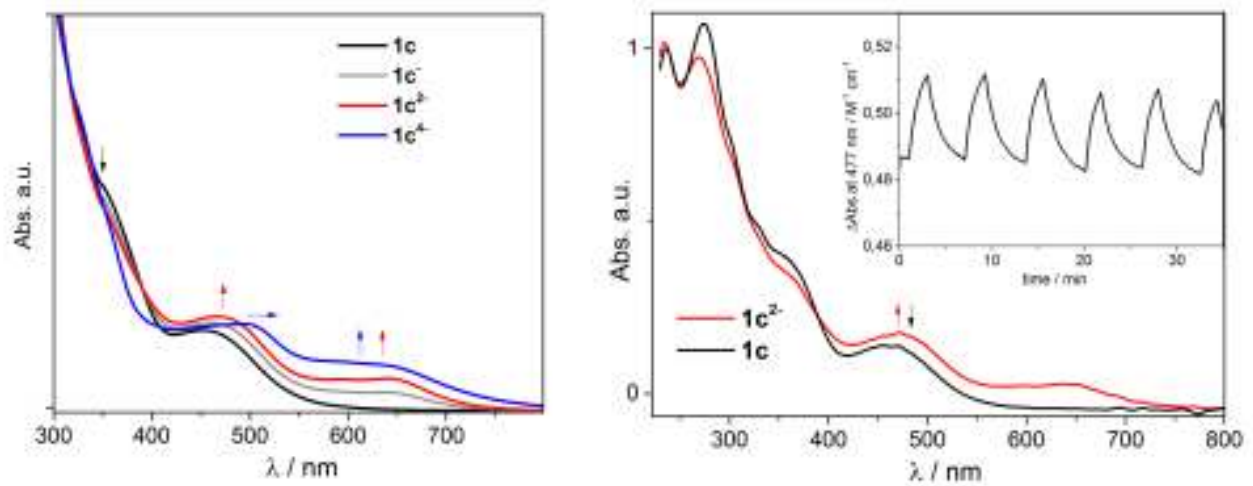

Figure 7. Left: Evolution of the UV-vis spectrum of **1c** upon successive reduction steps. Right: **1c** ↔ **1c**$^{2-}$ UV-vis switching within the whole spectral region and at 477 nm (insert) by applying 0 to -0.4 V *vs.* SCE (dichloromethane, 0.1 M Bu_4NPF_6).

The redox-triggered ECD modulation of *P*- and *M*-**1c** was then investigated. Accordingly, the ECD responses of both enantiomers were recorded while applying increasing potentials ranging from 0 to -0.4 V *vs.* SCE and gave expected mirror-image ECD changes (see Figure 8). For instance, *P*-**1c** displays a significant intensity decrease of the band at 470 nm accompanied by an increase in the signal at 350 nm with a distinct isobestic point at 410 nm. Interestingly, the negative Cotton effect observed at 407 nm for *P*-**1c** disappears when going to *P*-**1c**$^{2-}$. This is not unexpected as reduction of **1c** must predominantly occur at the electron-accepting TCBD moieties, thus affecting their π-electron system and consequently low-energy π-π* ICT helicene→TCBDs excitations and exciton coupling interactions between them. In addition, no ECD-active band was observed between 550 and 750 nm, contrary to the UV-vis response of **1c**$^{2-}$. We then evaluated the chiroptical switching activity of *M*-**1c** by successively applying potentials of 0.1 and -0.4 V *vs.* SCE during several cycles while recording its ECD response at 477 nm (Figure 8, insert). It showed a reversible Δε amplitude change between -30 and -24 M^{-1} cm^{-1} corresponding to *M*-**1c** and *M*-**1c**$^{2-}$, respectively, which last for more than 5 redox cycles, thus confirming the bistability of this new example of redox-triggered chiroptical switch.

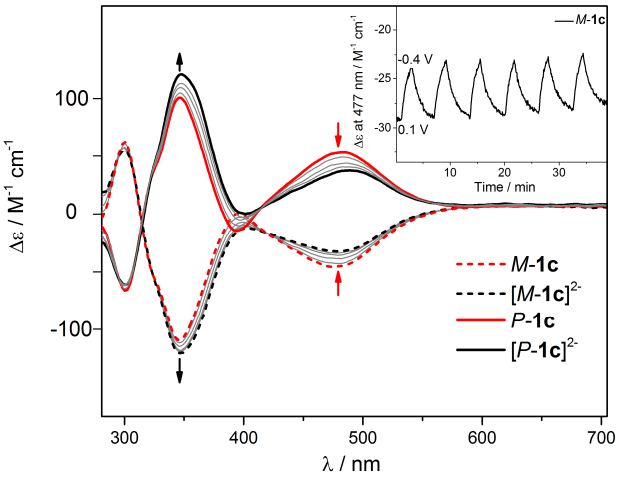

Figure 8. Modification of the ECD spectra of *M* and *P* enantiomers of **1c** upon 2e$^-$ reduction at -0.4 V (*vs.* SCE) and oxidation at +0.1 V (dichloromethane, 0.1 M Bu_4NPF_6). Insert: Tuning of the ECD response at 477 nm.

TPA spectroscopy

The Nonlinear Optical (NLO) activity of helicenes has been reported since a long time, especially in the case of second-order NLO effects and Second Harmonic Generation (SHG).[19] More recently, the two-photon absorption of helicenes has also been examined, together with the related two-photon circular dichroism.[8] These studies on organic helicenes derivatives have highlighted the effects of charge transfers (either internal to the helical backbone or external to it) and of the π-conjugation extension. Therefore, it appeared interesting to study the TPA response of our helicene-TCBD derivatives displaying significant charge transfer. The experimental and simulated (CAM-B3LYP *in vacuo*) TPA spectra and corresponding calculated TPA electronic transitions for **1b** and **1c** are presented in Figure 9. Regarding the experimental σ_{TPA} cross-section values, they range between 5-40 GM for mono-substituted **1b**, i.e. very similar to former helicene derivatives, namely 2-cyano-carbo[6]helicene,[8a] displaying significant intramolecular charge transfer. Bis-substituted helicene **1c** displays σ_{TPA} between 1-6 GM, i.e. much less than for **1b**. This difference can be justified based on previous work done by Brédas and co-workers.[20a] These authors demonstrated that in non-centrosymmetric conjugated molecules, with push-pull motif, a reduction of the permanent dipole moment can result in a reduction of the effective σ_{TPA}. This is the case in compound **1c**, where the relatively symmetric charge transfer around the central helicene core (Figure 2b) affects, directly, the difference in permanent dipole moments between the ground and excited states. In order to obtain the best theoretical-experimental match, the calculated spectra were -86 nm and -64 nm shifted for **1b** and **1c**, respectively; this is common practice in theoretical-experimental works.[21-25] First, we note the reasonable theoretical

reproduction of the experimental spectral shape of both **1b** and **1c**. The experiment shows the most intense measureable band at 690 nm for both molecules. Interestingly, while this peak corresponds to a transition to the first excited state for **1b**, it corresponds to the second for **1c**. This observation can be explained by comparing the dipolar symmetry of **1b** with the quadrupolar symmetry of **1c**, and acknowledging the non-planarity of the latter. In this scenario, it is not totally unexpected that TPA transitions in **1c** appear at longer wavelengths as a result of the intramolecular charge transfer from the donor to the acceptor along a quadrupolar path.[20b-d] In fact, the calculated spectrum of **1c** reveals a shoulder produced by the first excited state transition that was resolvable experimentally and measured around 730 nm. The less intense band predicted by the theory around 640 nm corresponds to the second and fourth excited state transitions for **1b** and **1c**, respectively. The band was measureable for **1b** and detectable for **1c**. However, the sharp increase in the experimental TPA below 600 nm, attributed to enhancement due to linear absorption likely explains why the 640 nm peak was not resolved for **1c**. A second important observation is that in the case of **1c** the predicted cross-sections are larger than the experimental. While difficult to explain this difference considering that all measurements were made in the femtosecond regime where excited state absorption is negligible,[26,27] it is a common observation in theoretical-experimental studies.[8,22-24,28-30] However, in the case of **1b**, the experimental cross-sections are almost exactly as predicted. The experimental differences could be attributed to the increased degree of symmetry found in **1c** compared to **1b**. The difference between the calculated and experimental cross-section of **1c** is more difficult to explain, perhaps solvent effects are more important in **1c** than in **1b** due to the quadrupolar ICT path.[20d] Finally, the experimentally observed strong TPA signal on the blue-side of the spectra is attributed to the enhanced TPA typically observed as the excitation wavelength approaches the linear absorption region.[31,32]

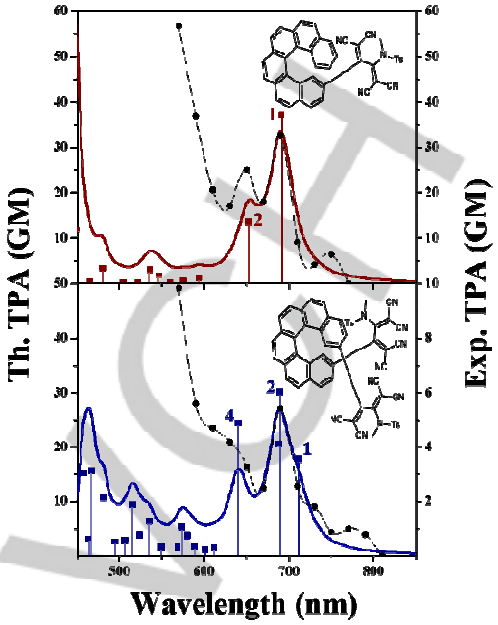

Figure 9. Experimental (black) and simulated TPA spectra along with calculated electronic transitions of **1b** (top, red, -86 nm shifted) and **1c** (bottom, blue, -64 nm shifted). See Experimental section for the corresponding theoretical and experimental details.

Conclusions

We have shown that grafting electron-withdrawing groups such as tetracyanobutadiene derivatives onto an enantiomerically pure carbo[6]helicene strongly modifies its electronic and (chir)optical properties. The strong charge transfers from the helicene core to the TCBD units result in the appearance of new absorption bands in the visible region, which are also strongly active in ECD spectroscopy. By comparing the bis-substituted system **1c** with former results on carbo[6]helicene grafted with two ethynyl-DPP units, we highlighted here a case of exciton coupling involving charge-transfer excitations which originate in the helicene π-system. This aspect of generating a strong ECD response from exciton coupling in symmetrical π-helical push-pull systems is very promising for future development of highly responsive chiral materials. Therefore, these two helicene push-pull systems emerge as complementary ones for future applications. Indeed, since the helicene-DPP units are strongly emissive and display good CPL activity, they may find applications as chiral emitters for bioimaging or in chiral OLEDs technology. On the contrary, the helicene-TCBD compounds are not emissive but display strong charge transfers, and may therefore be useful for charge transport applications or as chiral electron-accepting platforms for chiral sensing. Furthermore, two-photon absorption was also measured for **1b** and **1c** and was found higher is **1b** than in **1c**, due to symmetry considerations. Comparison of experimental two-photon circular dichroic responses between these two derivatives will be performed in the near future. Finally, we showed that grafting electron-accepting substituents such as TCBDs can give access to new types of redox-triggered chiroptical switches.

Experimental Section

Computational details for UV-vis and ECD

Time-dependent density functional theory (TDDFT) linear response calculations[15] of 120 lowest singlet excitation energies along with the associated dipole and rotatory strengths were performed using the BHLYP[33] exchange-correlation functional and a split-valence basis set with one set of polarization functions for non-hydrogen atoms, SV(P),[34] preceded by DFT geometry optimizations at BP[35]/SV(P) level. All these computations were performed without imposing symmetry employing the Turbomole package (TM6.6).[36] Solvent effects (dichloromethane, ε = 8.9) were included in the calculations via the conductor-like screening model (COSMO) with the default parameters of the TM6.6/COSMO implementation.[37] The simulated UV-vis and ECD spectra shown are the sums of Gaussian functions centered at the vertical excitation energies and scaled using the calculated dipole and rotatory strengths, with the root mean square width of σ = 0.2 eV.[38] Simulated spectra for the helicene-TMS precursor **2c** were taken from Dhbaibi *et al*.[14a]

Theoretical and experimental methods for TPA

The theoretical approach employed here was based on the success of the approach used in previous studies of this class of molecules.[8a,39,40] The molecular structures of **1b** and **1c** were DFT-optimized using the B3LYP[33b,41] hybrid functional with the 6-311G(d,p)[42,43] basis set in Gaussian 09.[44] TDDFT calculations of 20 excited states for each molecule were performed with the CAM-B3LYP[45] using the aforementioned basis set for **1b** and 6-31G(d)[42,43] for **1c** in Dalton 2013.[46] TPA spectra were calculated using: [47,48]

$$\delta_{0f}^{TPA}(\omega) = \frac{4\pi^3 \alpha a_0^5}{c} \sum_f (\hbar\omega_f)^2 \, \overline{\delta}_{0f}^{TPA}\left(\omega_{0f}\right) g(2\omega, \omega_{0f}, \Gamma), \quad (1)$$

$$\delta_{0f}^{TPA}(\omega) \approx 1.25273 \times 10^{-2} \times \omega^2 \sum_f g(2\omega, \omega_{0f}, \Gamma) \cdot \overline{\delta}_{0f}^{TPA}\left(\omega_{0f}\right) \quad (2)$$

Where c is the speed of light in vacuum, a_0 is the Bohr's radius, α is the fine structure constant, $E = \hbar\omega$ is the photon energy (half of the transition energy for the degenerate case), $\overline{\delta}_{0f}^{TPA}\left(\omega_{0f}\right)$ is the orientational averaged two-photon probability for the degenerate case and ω is the excitation frequency. A normalized Lorentzian lineshape function ($g\left(2\omega, \omega_{0f}, \Gamma\right)$) was used to broaden electronic transitions:

$$g(2\omega, \omega_{0f}, \Gamma) = \frac{1}{\pi} \frac{\Gamma_{gf}/_2}{(\omega_{gf} - 2\omega)^2 + (\Gamma_{gf}/_2)^2} \quad (3)$$

Here Γ is the FHWM linewidth for all transitions, in this specific case, 0.07 and 0.08 eV for **1b** and **1c**, respectively, to best fit experimental spectra. The calculated TPA spectra are in Göppert-Mayer units (GM), i.e. $10^{-50} cm^4 \cdot s \cdot molec^{-1} \cdot photon^{-1}$ when atomic units are used for the elements in Eqs. (1) and (2).

TPA measurements were performed on dichloromethane solutions with concentrations of 0.0025 M and 0.015 M for **1b** and **1c**, respectively, using the open aperture z-scan technique.[49,50] Two-photon excitation was induced with a computer-controlled femtosecond optical parametric amplifier (OPerA Solo) pumped by a COHERENT amplified laser system. The system is capable of generating 90 fs (FWHM) pulses from 240 nm to 2.6 μm with pulse energies up to 350 μJ. Experiments were performed using a 50 Hz repetition rate to avoid possible contribution from cumulative effects.

Acknowledgements

We thank the Ministère de l'Education Nationale, de la Recherche et de la Technologie, the Centre National de la Recherche Scientifique (CNRS), the University of Rennes 1 and the Ecole Nationale Supérieure de Chimie de Rennes. M.S.-H. acknowledges the young researchers' T-subsidy from the Ministry of Science and Higher Education in Poland. J. A. acknowledges National Science Foundation Grant CHE-1560881 and the Center for Computational Research in Buffalo for providing computing resources.

Keywords: helicene • tetracyanobutadiene • chiroptical activity • charge transfer • two-photon absorption

[1] *Chirality at the Nanoscale, Nanoparticles, Surfaces, Materials and more (Ed.: D. Amabilino)*. Wiley-VCH: **2009**.

[2] N. Harada, K. Nakanishi, N., Berova, *Electronic CD Exciton Chirality Method: Principles and Applications, in Comprehensive Chiroptical Spectroscopy: Applications in Stereochemical Analysis of Synthetic Compounds, Natural Products, and Biomolecules, Volume 2*, 4th ed.; John Wiley & Sons: New Jersey, **2012**.

[3] J. R. Brandt, F. Salerno, M. J. Fuchter, *Nature Rev. Chem.* **2017,** *1*, 0045.

[4] C. -F. Chen, Y. Shen, *Helicenes Chemistry: From Synthesis to Applications*. Springer, Berlin: **2017**.

[5] a) Y. Yang, R. C. da Costa, D.-M. Smilgies, A. J. Campbell, M. J. Fuchter, *Adv. Mater.* **2013**, *25*, 2624-2628; b) J. R. Brandt, X. Wang, Y. Yang, A. J. Campbell, M. J. Fuchter, *J. Am. Chem. Soc.* **2016,** *138* , 9743-9746.

[6] Y. Yang, R. C. da Costa, M. J. Fuchter, A. J. Campbell, *Nature Photonics* **2013**, *7*, 634-638.

[7] P. Josse, L. Favereau, C. Shen, S. Dabos-Seignon, P. Blanchard, C. Cabanetos, J. Crassous, *Chem. Eur. J.* **2017**, *23*, 6277-6281.

[8] a) C. Díaz, Y. Vesga, L. Echevarria, I. G. Stará, I. Starỳ, E. Anger, C. Shen, M. El Sayed Moussa, N. Vanthuyne, J. Crassous, A. Rizzo, F. E. Hernández, *RSC Adv.* **2015**, *5*, 17429-17437; b) Y. Vesga, C. Diaz, J. Crassous, F. E. Hernandez, *J. Phys. Chem. A* **2018**, *122*, 3365-3373.

[9] H. Isla, J. Crassous, *C. R. Chimie* **2016**, *19*, 39-49.

[10] a) T. Shoji, S. Ito, *Chem. Eur. J.* **2017**, *23*, 16696-16709; b) T. Michinobu, F. Diederich, *Angew. Chem. Int. Ed.* **2018**, *57*, 3552-3577; c) X. Wu, J. Wu, Y. Liu, A. K. Y. Jen, *J. Am. Chem. Soc.* **1999**, *121*, 472-473; d) T. Mochida, S. Yamazaki, *J. Chem. Soc. Dalton Trans.* **2002**, 3559-3564; e) Y. Morioka, N. Yoshizawa, J.-i. Nishida, Y. Yamashita, *Chem. Lett.* **2004**, *33*, 1190-1191; f) T. Michinobu, J. C. May, J. H. Lim, C. Boudon, J.-P. Gisselbrecht, P. Seiler, M. Gross, I. Biaggio, F. Diederich, *Chem. Commun.* **2005**, 737-739; g) T. Shoji, S. Ito, K. Toyota, M. Yasunami, N. Morita, *Chem. Eur. J.* **2008**, *14*, 8398-8408; h) T. Shoji, J. Higashi, S. Ito, T. Okujima, M. Yasunami, N. Morita, *Chem. Eur. J.* **2011**, *17*, 5116-5129; i) D. Koszelewski, A. Nowak-Krol, D. T. Gryko, *Chem. Asian J.* **2012**, *7*, 1887-1894; j) S.-i. Kato, H. Noguchi, S. Jin, Y. Nakamura, *Asian J. Org. Chem.* **2016**, *5*, 246-256.

[11] a) M. Kivala, F. Diederich, *Acc. Chem. Res.* **2009**, *42*, 235-248; b) S.-i. Kato, F. Diederich, *Chem. Commun.* **2010**, *46*, 1994-2006; c) T. Shoji, S. Ito, *Chem. Eur. J.* **2017**, *27*, 16696-16709; d) R. Garcia, J. Calbo, R. Viruela, M. A. Herranz, E. Orti, N. Martin, *ChemPlusChem* **2018**, *83*, 300-307; for an example of chiral butadiene system, see: e) M. Chiu, B. H. Tchitchanov, D. Zimmerli, I. A. Sanhueza, F. Schoenebeck, N. Trapp, W. B. Schweizer, F. Diederich, *Angew. Chem. Int. Ed.* **2015**, 54, 349-354.

[12] a) M. Betou, N. Kerisit, E. Meledje, Y. R. Leroux, C. Katan, J.-F. Halet, J.-C. Guillemin, Y. Trolez, *Chem. Eur. J.* **2014**, *20*, 9553-9557; b) M. Betou, R. J. Durand, A. Sallustrau, C. Gousset, E. Le Coz, Y. R. Leroux, L. Toupet, E. Trzop, T. Roisnel, Y. Trolez, *Chem. Asian J.* **2017**, *12*,

1338-1346; c) Y. Zhang, R. P. Hsung, M. R. Tracey, K. C. M. Kurtz, E. L. Vera, *Org. Lett.* **2004**, *6*, 1151-1154.

[13] a) M. El Sayed Moussa, K. Guillois, W. Shen, R. Réau, J. Crassous, C. Lescop, *Chem. Eur. J.* **2014**, *20*, 14853-14867; b) E. Anger, M. Srebro, N. Vanthuyne, L. Toupet, S. Rigaut, C. Roussel, J. Autschbach, J. Crassous, R. Réau, *J. Am. Chem. Soc.* **2012**, *134*, 15628-15631.

[14] a) K. Dhbaibi, L. Favereau, M. Srebro-Hooper, M. Jean, N. Vanthuyne, F. Zinna, B. Jamoussi, L. Di Bari, J. Autschbach, J. Crassous, *Chem. Sci.* **2018**, *9*, 735-742; b) Y. Si, G. Yang, *J. Mater. Chem. C* **2013**, *1*, 2354-2361; c) C. Liu, Y. Si, X. Pan, and G. Yang, *RSC Adv.* **2015**, *5*, 72907-72915; d) P. E. Reyes-Gutierrez, M. Jirasek, L. Severa, P. Novotna, D. Koval, P. Sazelova, J. Vavra, A. Meyer, I. Cısarova, D. Saman, R. Pohl, P. Stepanek, P. Slavıcek, B. J. Coe, M. Hajek, V. Kasicka, M. Urbanova, F. Teply, *Chem. Com.* **2015**, *51*, 1583-1586.

[15] a) J. Autschbach, *Chirality* **2009**, *21*, E116-E152; b) M. Srebro-Hooper, J. Autschbach, *Annu. Rev. Phys. Chem.* **2017**, *68*, 399-420.

[16] a) L. Cupellini, S. Jurinovich, M. Campetella, S. Caprasecca, C. A. Guido, S. M. Kelly, A. T. Gardiner, R. Cogdell, B. Mennucci, *J. Phys. Chem. B* **2016**, *120*, 11348-11359; b) J. D. Spiegel, I. Lyskov, M. Kleinschmidt, C. M. Marian, *Chem. Phys.* **2017**, *482*, 265-276; c) X. Li, R. M. Parrish, F. Liu, S. I. L. Kokkila Schumacher, T. J. Martínez, *J. Chem. Theory Comput.* **2017**, *13*, 3493-3504.

[17] a) P. M. Bayley, E. B. Nielsen, J. A. Schellman, *J. Phys. Chem.* **1969**, *73*, 228-243; b) M. Rudolph, J. Autschbach, *J. Phys. Chem. A* **2011**, *115*, 2635-2649.

[18] a) D. Schweinfurth, M. Zalibera, M. Kathan, C. Shen, M. Mazzolini, N. Trapp, J. Crassous, G. Gescheidt, F. Diederich, *J. Am. Chem. Soc.* **2014**, *136*, 13045-13052; b) J. R. Brandt, L. Pospısil, L. Bednarova, R. Correa da Costa, A. J. P. White, T. Mori, F. Teply, M. J. Fuchter, *Chem. Comm.* **2017**, *53*, 9059-9062; c) N. Saleh, N. Vanthuyne, J. Bonvoisin, J. Autschbach, M. Srebro-Hooper, J. Crassous, *Chirality* **2018**, *30*, 592-601.

[19] a) T. Verbiest, S. Van Elshocht, M. Kauranen, L. Hellemans, J. Snauwaert, C. Nuckolls, T. J. Katz, A. Persoons, *Science* **1998**, *282*, 913-915; b) A. Bossi, E. Licandro, S. Maiorana, C. Rigamonti, S. Righetto, G. R. Stephenson, M. Spassova, E. Botek, B. Champagne, *J. Phys. Chem. C* **2008**, *112*, 7900-7907; c) B. J. Coe, D. Rusanova, V. D. Joshi, S. Sanchez, J. Vavra, D. Khobragade, L. Severa, I. Cisarova, D. Saman, R. Pohl, K. Clays, G. Depotter, B. S. Brunschwig, F. Teply, *J. Org. Chem.* **2016**, *81*, 1912-1920.

[20] a) T. Kogej, D. Beljonne, F. Meyers, J. W. Perry, S.R. Marder, J. -L. Brédas, *Chem. Phys. Lett.* **1998**, *298*, 1-6; b) M. Albota, et al., *Science* **1998**, *281*, 1653-1656; c) M. Rumi, J. E. Ehrlich, A. A. Heikal, J. W. Perry, S. Barlow, Z. Hu, D. McCord-Maughon, T. C. Parker, H. Röckel, S. Thayumanavan, S. R. Marder, D. Beljonne, J.-L. Brédas, *J. Am. Chem. Soc.* **2000**, *122*, 9500-9510; d) D. Cvejn, E. Michail K. Seintis, M. Klikar, O. Pytela, T. Mikysek, N. Almonasy, M. Ludwig, V. Giannetas, M. Fakis, F. Bureš , *RSC Adv.* **2016**, *6*, 12819-12828.

[21] C. Toro, L. De Boni, N. Lin, F. Santoro, A. Rizzo, F. E. Hernandez, *Chem. Eur. J.* **2010**, *16*, 3504-3509.

[22] C. Díaz, L. Echevarria, A. Rizzo, F. E. Hernández, *J. Phys. Chem. A* **2014**, 118, 940-946.

[23] C. Díaz, L. Echevarria, F. E. Hernández, *J. Phys. Chem. A* **2013**, 117, 8416-8426.

[24] C. Diaz, N. Lin, C. Toro, R. Passier, A. Rizzo, F. E. Hernández, *J. Phys. Chem. Lett.* **2012**, *3*, 1808-1813.

[25] N. Lin, F. Santoro, X. Zhao, C. Toro, L. De Boni, F. E. Hernández, A. Rizzo, *J. Phys. Chem. B* **2011**, *115*, 811-824.

[26] F. Wu, G. Zhang, W. Tian, W. Chen, G. Zhao, S. Cao, W. Xie, *J. Opt. A-Pure Appl. Op.* **2009,** *11*, 0652061.

[27] F. E. Hernández, K. D. Belfield, I. Cohanoschi, M. Balu, K. J. Schafer, *Appl. Opt.* **2004**, *43*, 5394-5398.

[28] J. Donnelly, Y. Vesga, F. E. Hernández, *Chem. Phys.* **2016**, 447, 19-23.

[29] Y. Vesga, F. E. Hernández, *J. Phys. Chem. A*, **2016**, *120*, 6774-6779 .

[30] J. A. Tiburcio-Moreno, J. Alvarado-Gil, C. Diaz, L. Echevarria, F. E. Hernández, *Chem. Phys. Lett.* **2013**, *583*, 160-164.

[31] M. A. C., Nascimento, Chem. Phys.**1983**, *74*, 51-66.

[32] M. M. Alam, M. Chattopadhyaya, S. Chakrabarti, A. Rizzo, *PhysChemChemPhys* **2014**, *16*, 8030-8035.

[33] a) A. D. Becke, *J. Chem. Phys.* **1993**, *98*, 1372-1377; b) C. Lee, W. Yang, R. G. Parr, *Phys. Rev. B* **1988**, *37*, 785-789.

[34] a) A. Schäfer, H. Horn, R. Ahlrichs, *J. Chem. Phys.* **1992**, *97*, 2571-2577; b) K. Eichkorn, F. Weigend, O. Treutler, R. Ahlrichs, *Theor. Chem. Acc.* **1997**, *97*, 119-124; c) F. Weigend, R. Ahlrichs, *Phys. Chem. Chem. Phys.* **2005**, *7*, 3297-3305.

[35] a) A. D. Becke, *Phys. Rev. A* **1988**, *38*, 3098-3100; b) J. P. Perdew, *Phys. Rev. B* **1986**, *33*, 8822-8824; c) J. P. Perdew, *Phys. Rev. B* **1986**, *34*, 7406.

[36] a) TURBOMOLE V6.6 2014, a development of University of Karlsruhe and Forschungszentrum Karlsruhe GmbH, 1989-2007, TURBOMOLE GmbH, since 2007; available from http://www.turbomole.com; b) R. Ahlrichs, M. Bär, M. Häser, H. Horn, C. Kölmel, *Chem. Phys. Lett.* **1989**, *162*, 165-169; c) F. Furche, R. Ahlrichs, C. Hättig, W. Klopper, M. Sierka, F. Weigend, *WIREs Comput. Mol. Sci.* **2014**, *4*, 91-100.

[37] a) A. Klamt, G. J. Schüürmann, *J. Chem. Soc., Perkin Trans. 2* **1993**, 799-805; b) A. Klamt, *J. Phys. Chem.* **1996**, *100*, 3349-3353.

[38] J. Autschbach, T. Ziegler, S. J. A. van Gisbergen, E. J. Baerends, *J. Chem. Phys.* **2002**, *116*, 6930-6940.

[39] F. E. Hernández, A. Rizzo, Molecules **2011**, *16*, 3315-3337.

[40] B. Jansík, A. Rizzo, H. Ågren, B. Champagne, *J. Chem Theory Comput.* **2008**, *4*, 457-467.

[41] A. D. Becke. *J. Chem. Phys.* **1993**, *98*, 5648-5652.

[42] R. Krishnan, J. S. Binkley, R. Seeger, J. A. Pople, *J. Chem. Phys.* **1980**, 72, 650-654.

[43] T. Clark, J. Chandrasekhar, G. W. Spitznagel, P. V. R. Schleyer, *J. Comput. Chem.* **1983**, *4*, 294-301.

[44] M. J. Frisch, G. W. Trucks, H. B. Schlegel, G. E. Scuseria, M. A. Robb, J. R. Cheeseman, G. Scalmani, V. Barone, B. Mennucci, G.A. Petersson, H., *et al.* Gaussian 09, Revision A.1. Gaussian, Inc., Wallingford CT, **2009**.

[45] T. Yanai, D. P. Tew, N. C. Handy, *Chem. Phys. Lett.* **2004**, *393*, 51-57.

[46] K. Aidas, C. Angeli, K. L. Bak, V. Bakken, R. Bast, L. Boman, O. Christiansen, R. Cimiraglia, S. Coriani, P. Dahle, E.K., *et al.* The Dalton Quantum Chemistry Program System. Wiley Interdiscip. *Rev. Comput. Mol. Sci.* **2014**, 4, 269.

[47] A. Rizzo, S. Coriani, K. Ruud, *Computational Strategies for Spectroscopy*, John Wiley & Sons, Inc., **2011**, p. 77-135.

[48] W. M. McClain, J. Chem. Phys. **1971**, 55, 2789-2796.

[49] M. Sheik-bahae, A. A. Said, E. W. Van Stryland, *Opt. Lett.* **1989**, *14*, 955-957.

[50] M. Sheik-Bahae, A. A. Said, T. H. Wei, D. J. Hagan, E. W. Van Stryland. *IEEE J. Quant. Electron.* **1990**, *26*, 760-769.

10.1002/chem.201802763

WILEY-VCH

Entry for the Table of Contents (Please choose one layout)

Layout 2:

FULL PAPER

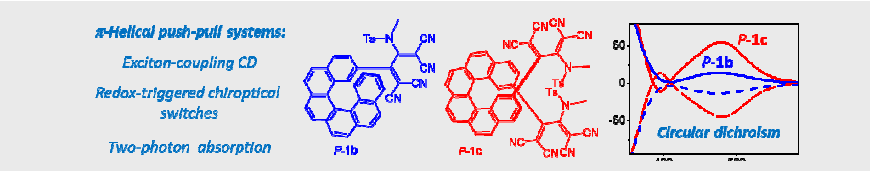

A new type of π-helical push-pull molecules has been prepared, consisting of helicene grafted with tetracyanobutadienes as accepting substituents.

R. Bouvier, R. Durand, L. Favereau, M. Srebro-Hooper, V. Dorcet, T. Roisnel, N. Vanthuyne, Y. Vesga, J. Donnelly, F. Hernandez, J. Autschbach, Y. Trolez,* and J. Crassous**

Page No. – Page No.

Helicenes grafted with 1,1,4,4-tetracyanobutadiene moieties: π-helical push-pull systems with strong electronic circular dichroism and two-photon absorption